



HAL
open science

Influence of surface and subsurface Co–Ir alloy on the electronic properties of graphene

Kangli Wang, Thomas Vincent, Jean Baptiste Bouhiron, Stephane Pons, Dimitri Roditchev, Sabina Simon, Mikhail Fonin, Beate Paulus, Yuriy Dedkov, Sergio Vlaic, et al.

► **To cite this version:**

Kangli Wang, Thomas Vincent, Jean Baptiste Bouhiron, Stephane Pons, Dimitri Roditchev, et al.. Influence of surface and subsurface Co–Ir alloy on the electronic properties of graphene. *Carbon*, 2021, 183, pp.251-258. 10.1016/j.carbon.2021.06.082 . hal-03365369

HAL Id: hal-03365369

<https://hal.science/hal-03365369>

Submitted on 5 Oct 2021

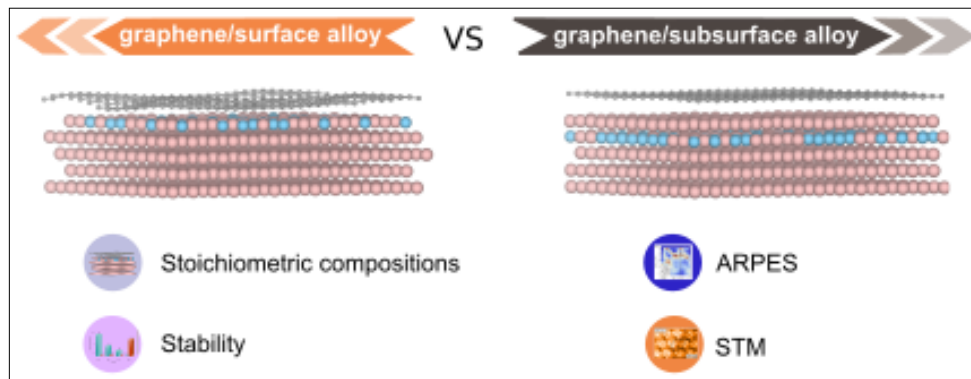
HAL is a multi-disciplinary open access archive for the deposit and dissemination of scientific research documents, whether they are published or not. The documents may come from teaching and research institutions in France or abroad, or from public or private research centers.

L'archive ouverte pluridisciplinaire **HAL**, est destinée au dépôt et à la diffusion de documents scientifiques de niveau recherche, publiés ou non, émanant des établissements d'enseignement et de recherche français ou étrangers, des laboratoires publics ou privés.

Graphical Abstract

Influence of surface and subsurface Co-Ir alloy on the electronic properties of graphene

Kangli Wang, Thomas Vincent, Jean Baptiste Bouhiron, Stephane Pons, Dimitri Roditchev, Sabina Simon, Mikhail Fonin, Beate Paulus, Yuriy Dedkov, Sergio Vlaic, Elena Voloshina



Highlights

Influence of surface and subsurface Co-Ir alloy on the electronic properties of graphene

Kangli Wang, Thomas Vincent, Jean Baptiste Bouhiron, Stephane Pons, Dimitri Roditchev, Sabina Simon, Mikhail Fonin, Beate Paulus, Yuriy Dedkov, Sergio Vlaic, Elena Voloshina

- The composition and position of CoIr alloy affects the graphene layer morphology
- The presence of Co at the interface tends to destroy the Dirac cone
- The Dirac cone is preserved if subsurface Co-Ir alloy is formed

Influence of surface and subsurface Co-Ir alloy on the electronic properties of graphene

Kangli Wang^a, Thomas Vincent^b, Jean Baptiste Bouhiron^{b,c}, Stephane Pons^b, Dimitri Roditchev^b, Sabina Simon^d, Mikhail Fonin^d, Beate Paulus^a, Yuriy Dedkov^{a,e,*}, Sergio Vlaic^{b,**}, Elena Voloshina^{a,e},

^a*Institut für Chemie und Biochemie, Freie Universität Berlin, Arnimallee 22, 14195 Berlin, Germany*

^b*Laboratoire de Physique et d'Étude des Matériaux, ESPCI Paris, PSL Research University, CNRS, UMR 8213, Sorbonne Universités, UPMC Univ. Paris 06, 75005 Paris, France*

^c*Laboratoire Kastler Brossel, Collège de France, CNRS, ENS-PSL University, Sorbonne Universités, 11 Place Marcelin Berthelot, 75005 Paris, France*

^d*Department of Physics, University of Konstanz, 78457 Konstanz, Germany*

^e*Department of Physics, Shanghai University, Shangda Road 99, 200444 Shanghai, China*

Abstract

Using density functional theory (DFT) calculations and angle-resolved photoemission spectroscopy (ARPES) the structural and electronic properties of graphene on the surface and subsurface Co-Ir alloy are investigated upon the intercalation of Co in graphene/Ir(111). It is found computationally that the interaction strength between graphene and substrate is strongly affected by the composition and nature of an alloy, implying the large difference in the electronic structure of monolayer graphene on $\text{Co}_x\text{Ir}_{1-x}/\text{Ir}(111)$ and $\text{Ir}/\text{Co}_x\text{Ir}_{1-x}/\text{Ir}(111)$. All theoretical results are supported by our ARPES

*Corresponding author

**Corresponding author

Corresponding author

Email addresses: yuriy.dedkov@icloud.com (Yuriy Dedkov), sergio.vlaic@espci.fr (Sergio Vlaic), elena.voloshina@icloud.com (Elena Voloshina)

data, which demonstrate the disappearance of the Dirac cone when graphene lies on Co and its restoration upon the formation of the subsurface Co-Ir alloy.

Keywords:

graphene, intercalation, alloy, DFT, LEED, STM, ARPES

1. Introduction

Since the first isolation of free-standing graphene (gr) and remarkable experiments on its transport properties in 2005 [1, 2], numerous studies have been conducted on graphene mainly due to its excellent electronic [3], thermal [4], and mechanical [5] properties. However, the low production output of the mechanical exfoliation method (which is usually used in the studies of transport properties of graphene) and its low scalability make it unavailable for the large scale production of graphene. Therefore, many approaches for synthesising graphene have been developed, such as epitaxial growth on SiC surfaces [6, 7, 8], reduction of graphene oxide [9, 10], and chemical vapor deposition (CVD) on metals and semiconductors [11, 12, 13, 14]. Among these strategies, the CVD of graphene on metals has become the most promising approach because of its inexpensive and large-scale preparation of high-quality graphene films [15, 16]. Moreover, it is found that the graphene-metal system is a very interesting object in itself [17, 18, 19, 20]. For example, the moiré structure is formed by graphene on a variety of metal substrates, such as Ir(111) [21, 22, 23, 24, 25, 26] and Ru(0001) [27, 28, 29, 30, 31] due to the relatively large lattice constant mismatch between graphene and substrate. More interestingly, the ferromagnetic substrates, such as Co(0001)

20 and Ni(111), induce magnetic polarisation in graphene and overlap with a graphene valence state in reciprocal space for one spin direction only [32, 33, 34, 35, 36], which are appealing properties for future spintronic devices [37].

Intercalation of different species, and particularly metal layers, in between graphene and substrate offers an effective route towards modifying the structural, electronic, and magnetic properties of graphene. For example, the single layer of Cu sandwiched between graphene and Ir(111) opens a band gap in the graphene π bands resulted from the hybridisation between the Cu and the carbon derived states [38]. Moreover, the implementation of magnetic ultra-thin films into the graphene-metal system, like gr/Co/Ir(111), allows achieving a remarkable enhancement of perpendicular magnetic anisotropy (PMA) via the interaction between graphene and the underlying magnetic metal thick film [39, 40, 41]. However, the intercalation of alloy in between graphene and substrate, which may bring new properties to graphene, is still largely unexplored [42, 43].

35 In this combined theoretical and experimental study, we gain a unique and detailed insight into the properties of graphene on surface alloy gr/Co_xIr_{1-x}/Ir(111) and subsurface alloy gr/Ir/Co_xIr_{1-x}/Ir(111). By performing the state-of-the-art first principles calculations, we explore how different compositions of surface and subsurface Co-Ir alloy influence the moiré structure, graphene-metal charge transfer, band structure, and stability of a graphene layer on Ir(111), and further compare them with the experimental results. The deeper insights into the interplay between graphene structure and different kinds of Co-Ir alloy from this study are expected to provide a useful guide for achieving precise layer controlled graphene growth and the

45 design of graphene-based devices.

2. Computational and Experimental Details

DFT calculations. The DFT calculations were carried out with the Vienna *ab initio* simulation package (VASP) [44, 45, 46], employing the generalised gradient approximation (GGA) functional of Perdew, Burke and
50 Ernzerhof (PBE) [47]. The van der Waals interactions were incorporated by the semi-empirical approach of Grimme through the D2 correction [48]. The ion-cores were described by projector-augmented-wave (PAW) potentials [49] and the valence electrons [C ($2s, 2p$), Ir ($5d, 6s$), Co ($3d, 4s$)] were described by plane waves associated to kinetic energies of up to 500 eV. A
55 Γ -centred $3 \times 3 \times 1$ k-point mesh was used. Due to the different lattice constants of graphene and metal support, the systems studied in the present work were modelled by a (10×10) graphene unit cell placed on a (9×9) cell of Ir(111) with the intercalation of Co-Ir alloy. The Co-Ir alloy is simulated by a $\text{Co}_x\text{Ir}_{1-x}$ layer after random replacing Ir atoms by Co atoms. In order
60 to prevent interlayer interaction within the periodic images, a vacuum spacing of 20 \AA was applied for all systems. Our slab geometry includes in total 605 atoms (1 layer of graphene, 1 layer of $\text{Co}_x\text{Ir}_{1-x}$ alloy and 4 layers of Ir) in the unit cell. The lattice constant in the lateral plane was set according to the optimised value of bulk metal ($a_{\text{Ir}(111)} = 2.723 \text{ \AA}$). The positions (x ,
65 y , z coordinates) of C atoms and intercalant as well as z -coordinates of the two topmost layers of the substrate were fully relaxed until the forces were smaller than 0.02 eV/\AA . The convergence criteria for energy was set equal to 10^{-5} eV . The STM images were calculated using the Tersoff-Hamann formal-

ism [50]. To recover an effective primitive cell band structure picture from
70 the supercell band structure, the BandsUP software was employed [51, 52].

Experiments. The same Ir(111) crystal was used in all experiments and
it has been cleaned in UHV environment by cycles of Ar⁺ sputtering at
1 keV and flash annealing at 1400 K. A graphene layer has been grown by
repeated cycles of temperature programmed growth (TPG) [21], exposing the
75 Ir surface to ethylene (partial pressure 2×10^{-7} mbar) at room temperature,
followed by a 1400 K flash for few seconds. Co has been deposited at 673 K
on the as prepared gr/Ir(111) surface when not specified elsewhere in the
main text, followed by a 30 min annealing to perform the intercalation. The
graphene coverage has been measured by scanning tunnelling microscopy
80 (STM) in one case and by Auger electron spectroscopy in the angle-resolved
photoemission spectroscopy (ARPES) chamber comparing the peak to peak
intensity of the Auger C *KVV* signal (272 eV) with respect to the one of
full graphene layer grown on Ir by exposing the surface of the sample to
 2×10^{-7} mbar of ethylene at 1400 K for 1 h [53].

85 STM and ARPES experiments have been performed in two separated
ultra-high vacuum (UHV) stations in identical experimental conditions al-
lowing the reproducibility of the sample preparation. Both experimental
stations are equipped with low energy electron diffraction (LEED). Base pres-
sure in both stations is $< 8 \times 10^{-11}$ mbar. ARPES measurements have been
90 performed with SPECS PHOIBOS 225-2D-CCD hemispherical analyser, us-
ing a *p*-polarised (90% degree of polarisation) He II discharge spectral line
($h\nu = 40.8$ eV) as a photon source. During ARPES measurements the sam-
ple was placed on the 6-axis fully motorised manipulator and was kept at

$T < 50$ K. STM experiments were carried with an Omicron VT STM in the
95 constant-current mode at room temperature using electrochemically etched
polycrystalline tungsten tips cleaned in UHV by flash annealing. The sign
of the bias voltage corresponds to the voltage at the sample. Tunnelling pa-
rameters are: $U_T = 1$ V for tunnelling voltage and $I_T = 1$ nA for tunnelling
current.

100 **3. Results and Discussion**

3.1. Theoretical analysis

To understand how the different stoichiometric compositions of $\text{Co}_x\text{Ir}_{1-x}$
alloy influence the morphological structure of the gr/Co-Ir interface, five val-
ues for the ratio $x = 0.00, 0.25, 0.50, 0.75, 1.00$ are considered with a random
105 distribution of the Co atoms in the alloy. Moreover, surface and subsurface
alloys: $\text{Co}_x\text{Ir}_{1-x}$, $\text{Co}_x\text{Ir}_{1-x}/\text{Co}_x\text{Ir}_{1-x}$ and $\text{Ir}/\text{Co}_x\text{Ir}_{1-x}$ on Ir(111) substrate are
used to absorb the graphene layer. The summary of theoretical results for all
studied systems are presented in TableS1 of Supporting Information. Here
we only focus on the gr/ $\text{Co}_x\text{Ir}_{1-x}$ /Ir(111) and gr/Ir/ $\text{Co}_x\text{Ir}_{1-x}$ /Ir(111) sys-
110 tems. The corresponding structures obtained after full relaxation of atomic
positions are displayed in Figure 1.

In considerations of graphene on close-packed metal surfaces, several high
symmetry positions are usually identified: ATOP, FCC, and HPC (Fig. 1(a)),
which are surrounded by a carbon ring with respect to the adsorption po-
115 sition [19]. From Figure 1(b)-(e) and TableS1 of Supporting Information
it can be clearly seen that an enhanced corrugation of the graphene moiré
superstructure is formed on the top of $\text{Co}_x\text{Ir}_{1-x}$ /Ir(111) compared to that on

Ir(111). For $x = 0.25$, the minimum distance between graphene and the first layer of the substrate is 3.017 \AA , indicating the physisorption of graphene on the substrate. As x increases, the average height of the graphene layer with respect to the first layer dramatically decreases. At the same time for large x , we observe the coexistence of physisorbed and chemisorbed graphene, depending on the lateral position of C atoms above the top layer of the substrate. The physisorbed regime dominated by the van der Waals interaction is mainly distributed around the ATOP site with $\Delta h > 3.0 \text{ \AA}$, resulting in the formation of local protrusions. In the chemisorbed case, a close adsorption distance reaches a value as low as $\approx 1.9 \text{ \AA}$ (1.883 \AA for $x = 0.50$, 1.895 \AA for $x = 0.75$ and 1.912 \AA for $x = 1.00$), since the p_z orbitals of C atoms hybridise strongly with the Co d orbitals. Therefore, the graphene corrugation becomes pronounced with the increase of x .

In contrast, the presence of subsurface alloy of Ir/Co $_x$ Ir $_{1-x}$ weakens the corrugation of the graphene layer compared to the gr/Ir(111) system as shown in Figure 1(f)-(i) and Table S1 of Supporting Information. In particular, the local protrusions around ATOP tend to be flat, leading to an indistinct moiré structure. For all cases of the gr/Ir/Co $_x$ Ir $_{1-x}$ /Ir(111) interface, the calculated distances between graphene and the first metal layer keep around 3.4 \AA and are characteristic of physisorbed graphene, which indicates that the interaction of graphene with Ir layer is rather weak. With the increase of x , there is no obvious change in the corrugation, suggesting the insensitivity of morphological structure to the subsurface alloy. Overall, on the basis of structural arguments, our calculations reveal that the position, as well as stoichiometric compositions of the Co-Ir alloy, drives the corrugation of the

graphene layer in the mismatched structures.

The interfacial charge density differences for gr/Co_xIr_{1-x}/Ir(111) and
145 gr/Ir/Co_xIr_{1-x}/Ir(111) are plotted in Figure S1 to deeper understand the
effects of surface and subsurface alloy on the morphological structure of
graphene. In the absence of Co-Ir alloy, there is a minor redistribution and
electronic polarisation between graphene and Ir(111). When the Co-Ir alloy
is present at the surface of Ir(111), the charge transfer between graphene and
150 substrate is much stronger than that between graphene and Ir(111). Further-
more, with the increase of x , the charge accumulation between graphene and
surface alloy increases significantly, resulting in the strong chemical bonds
between graphene and the Co-Ir alloy. As a result, the C-C bonds of graphene
on the Co_xIr_{1-x}/Ir(111) would be weaker than those on Ir(111). When the
155 Co-Ir alloy is buried under the top Ir layer, the charge density transferred
from the Ir surface layer to graphene is slightly reduced compared to the
gr/Ir(111) system due to the electronic structure effect of Co ($3d^74s^2$) and
Ir ($5d^76s^2$) atoms. The top view in Figure S1(f)-(i) shows that as the x in-
creases, the electronic polarisation of the alloy layer first enhances and then
160 weakens, reaching the maximum at $x = 0.5$. The less charge accumula-
tion between graphene and surface Ir induced by the subsurface alloy could
confine the out-of-plane deformation of graphene, and therefore, the C-C
bonds of graphene adsorbed on Ir/Co_xIr_{1-x}/Ir(111) are closer to those of
freestanding graphene. In summary, the surface Co-Ir alloy could enhance
165 the interfacial interaction between graphene and substrate, while the sub-
surface Co alloy weakens the interfacial interaction between graphene and
substrate (Fig. 2(a)), implying the big difference in the electronic structure

of monolayer graphene on $\text{Co}_x\text{Ir}_{1-x}/\text{Ir}(111)$ and $\text{Ir}/\text{Co}_x\text{Ir}_{1-x}/\text{Ir}(111)$.

In order to assess the stability of the considered systems, we compare the
170 total energies of $\text{gr}/\text{Co}_x\text{Ir}_{1-x}/\text{Ir}(111)$ and $\text{gr}/\text{Ir}/\text{Co}_x\text{Ir}_{1-x}/\text{Ir}(111)$ and further
obtain the energy difference (ΔE) per atom as a function of x ratio as illus-
trated in Figure 2(b). At $x = 0.25$, the $\text{gr}/\text{Ir}/\text{Co}_x\text{Ir}_{1-x}/\text{Ir}(111)$ is energeti-
cally more favourable than $\text{gr}/\text{Co}_x\text{Ir}_{1-x}/\text{Ir}(111)$ by 9.4 meV per atom, despite
the interaction between graphene and the first layer in $\text{gr}/\text{Ir}/\text{Co}_x\text{Ir}_{1-x}/\text{Ir}(111)$
175 is much weaker than that in $\text{gr}/\text{Co}_x\text{Ir}_{1-x}/\text{Ir}(111)$. As the x value increases,
the $\text{gr}/\text{Ir}/\text{Co}_x\text{Ir}_{1-x}/\text{Ir}(111)$ is consistently more stable, but the total energy
difference per atom significantly decreases: $\Delta E = 4.3$ meV for $x = 0.50$
and $\Delta E = 2.2$ meV for $x = 0.75$. However, when the x increases to 1, the
energy difference has an opposite trend, where the $\text{gr}/\text{Ir}/\text{Co}_x\text{Ir}_{1-x}/\text{Ir}(111)$
180 system is energetically unfavourable by 7.3 meV per atom. We attribute
this phenomenon mainly to the following joint effects: (1) the interaction
between the top layer of the substrate and the graphene layer and (2) the
deformation energy of graphene. More specifically, at a low Co concentra-
tion, the interaction between the graphene layer and the surface Co-Ir alloy
185 is insufficient to overcome the deformation of graphene, consequently form-
ing a subsurface alloy underneath the gr/Ir interface bilayer. With the in-
creases of x , more chemical bonds are constructed between graphene and
Co-Ir alloy in system of $\text{gr}/\text{Co}_x\text{Ir}_{1-x}/\text{Ir}(111)$, thereby stabilising its system
and further reducing the energy difference between $\text{gr}/\text{Co}_x\text{Ir}_{1-x}/\text{Ir}(111)$ and
190 $\text{gr}/\text{Ir}/\text{Co}_x\text{Ir}_{1-x}/\text{Ir}(111)$. When the x reaches a certain value, the interaction
between graphene and surface alloy is strong enough to overcome the defor-
mation of a graphene monolayer and therefore the alloy tends to exist on the

surface under graphene. Our structure and stability analysis also confirms that the selective tuning of the Co concentration enables modifying the moiré
195 superstructure of graphene via changing the position of alloy in gr/Ir(111).

To characterise the changes in the electronic structure induced by Co-Ir alloy intercalation, we performed spin-polarised band structure calculation for gr/Co_xIr_{1-x}/Ir(111) and gr/Ir/Co_xIr_{1-x}/Ir(111). The results are presented in Figure 3 and Figure S2. Due to the weak interaction between graphene
200 and Ir(111), the band structure of gr/Ir(111) has quasi freestanding character where graphene is *p*-doped with the Dirac point located at 0.11 eV above E_F (Fig. S2(a) and Fig. 3(a)). Also, a band gap of 0.22 eV is opened at the Dirac point as a result of the hybridisation of the graphene-derived π and valence band states of Ir, which agrees well with the previous study of
205 0.2...0.3 eV [19, 54, 55]. Formation of a Co_{0.25}Ir_{0.75} alloy at the gr-Ir interface yields some changes in the graphene-derived band structure (Fig. S2(b) and Fig. 3(b)). Firstly, the presence of Co leads to small downward shift of both the π and σ states due to the electron donation from Co to the graphene π states. Then, symmetry breaking caused by random distribution of Co and
210 Ir in the interface layer, leads to somewhat blurring of the energy bands. As a consequence, one cannot unequivocally detect formation of the energy gap at the Dirac point, although the linear dispersion of π -bands is clearly visible. Further increase of Co concentration in the surface alloy results in complete violation of the Dirac cone as well as linear dispersion of π states
215 due to the large overlap of the C p_z states and Co d states (Fig. S2(c)). With increasing x to 0.5 the blurring of the energy bands also increases. In addition, new π and σ states appear accompanied by the original one. As the

x value becomes 1, the band structure of gr/Co/Ir(111) is similar to that of gr/Co_{0.5}Ir_{0.5}/Ir(111) with one exception that the band structure evolves clearly and the π and σ states exhibit a clear shift toward more negative energy (Fig. S2(d)).

When graphene is adsorbed on Ir/Co _{x} Ir_{1- x} /Ir(111), the dispersion of the graphene-derived π state in the vicinity of the K point and Dirac cone can still be clearly identified for $x = 0.5$ and $x = 1$ (Fig. 3(c) and (d)). In the case of complete Co monolayer (i. e. $x = 1$), a clear p -doping of a graphene layer is detected with the calculated position of the Dirac point of $E_D - E_F = 0.27$ eV and $E_D - E_F = 0.18$ eV for spin-up and spin-down channels, respectively. Furthermore, one can observe the existence of the energy gap of 0.20 eV in the energy dispersion of the π -band (Fig. 3(c)). For $x = 0.5$, graphene derived π -bands are slightly blurred, that does not allow to determine clearly neither position of Dirac point nor the band gap width (Fig. 3(d)). Still, quasi freestanding character of a p -doped graphene is undoubted. We also note that even though a complete monolayer of Co is present at the subsurface, the graphene π band at the K point is weakly spin-polarised with 0.09 eV energy splitting (Fig. 3(d)).

3.2. Experimental results

The experimental verification of the theoretical predictions reported in this work requires an excellent control of the Co-Ir alloy formation below the graphene layer. Since the graphene growth requires high temperatures (typically above 1000 K [56, 19]), at which a previously adsorbed Co thin film will desorb from the metallic substrate, the experimental realisation of the proposed systems has been achieved by intercalation technique of Co be-

tween graphene and Ir(111) substrate. In such systems Co can intercalates
by thermal annealing both through the defects in the graphene layer and
245 at the graphene flakes edges, the efficiency of the two intercalation mecha-
nisms can be controlled by the sample preparation conditions [57, 58]. It
has been demonstrated that the intermixing between Co and Ir atoms starts
at temperatures of above 773 K [59, 60]. To control the onset of the al-
loy formation, we therefore fixed the Co intercalation temperature to 673 K,
250 *i. e.* below the intermixing temperature, and the alloying has been achieved
by a further annealing to 873 K. Due to the reduced mobility of Co atoms
under graphene [61], the graphene layer has been grown by temperature
programmed growth (TPG) [21] ensuring the presence of a high density of
nanometric holes necessary to perform the intercalation from the side of the
255 graphene flake. Figure S3 (a) and (b) in Supporting Information demonstrate
the efficiency of this procedure and the absence of Co-Ir alloying upon in-
tercalation. The graphene layer becomes strongly corrugated (corrugation
of about 0.1 nm) as expected for the Co intercalated graphene (see Fig. S3
of Supporting Information for the STM simulations and Refs. 40, 61. The
260 presence of nanometric holes in the graphene layer results only in a broaden-
ing of its bands dispersions observed in the photoemission data by a factor
of ≈ 1.5 [22], which, within our resolution, is equivalent to the one of a
complete graphene layer grown by standards CVD technique [53] as shown
in Figure S3(c)-(f) of Supporting Information. These properties makes our
265 sample preparation method ideal for the present study.

In order to identify the electronic dispersion originating from the interca-
lated Co layer and its effect on the graphene dispersion, we first present the

electronic properties of the bare Ir(111) substrate along the $M_{gr}-K_{gr}-\Gamma$ di-
 rection (see Fig. 4(a,b)). Here, three Ir-derived surface states, named $S1$, $S2$
 270 and $S3$, are easily recognisable. Another electronic band, named I according
 to refs [62, 63], is weakly dispersing. At the K_{gr} point the $S2$ and $S3$ states
 become barely distinguishable, while the I state moves to higher binding en-
 ergy. The effect of the 1 ML deposition of Co at room temperature on bare
 Ir(111) is showed in Figure 4(c). Co grows pseudomorphic to Ir, as seen by
 275 the LEED diffraction pattern shown as inset, modifying the electronic dis-
 persion. Along the $K_{gr}-\Gamma$ direction a new state, dispersing similarly to the
 I state, appears at a lower binding energy (≈ 100 meV). Along the $M_{gr}-K_{gr}$
 direction, this new states mimics the dispersion of the $S3$ state. From these
 data, it is possible to conclude that Co electrons hybridize with the Ir(111)
 280 surface states and the I state leading to the new CoI state making it a clear
 indicator of the structural quality of the Co-Ir interface.

Figure 4(d) shows the effect of 1 ML Co intercalation between graphene
 (covering 75% of the surface as shown in Supplemental Informations) and
 Ir(111). Here the Co has been deposited at 673 K assuring intercalation but
 285 avoiding any alloy with the Ir substrate. In agreement with our theoretical
 calculations, the graphene Dirac cone vanishes from the Fermi level while
 the CoI state can be easily detected. The LEED pattern, shown as inset,
 demonstrates the presence of graphene through the typical moiré diffraction
 pattern of graphene on metals with high lattice mismatch.

290 According to our calculations, the subsurface Co-Ir alloy is energetically
 favorable at low Co concentration. To test the effect of such configuration
 on the electronic properties of the system we first intercalated 0.5 ML of Co

between graphene (75% coverage) and Ir(111) by Co deposition at 673 K. The electronic dispersion of such sample is shown in Figure 4(e). The *Co1* state and the graphene Dirac cone can be easily identified. Moreover the

 295 graphene Dirac cone can be fitted by a tight binding model up to the third nearest neighbour (red dashed lines). The excellent agreement, as expected for quasi-freestanding graphene [64], of the fit demonstrates that our sample is composed of regions of gr/Ir(111) and regions of gr/Co/Ir(111). A further

 300 annealing to 873 K dramatically changes the electronic dispersion (Fig. 4(f)) via the formation of the Co-Ir alloy. Along the $M_{\text{gr}}-K_{\text{gr}}$ direction the dispersion of the *Co1* state is clearly modified. Moreover the Dirac cone, although still present at the Fermi level, shrinks and its dispersion changes with respect the tight binding model. The strong enhancement of all the band width

 305 is probably due to the formation of Co-Ir alloy with a random stoichiometry but the presence of the graphene Dirac cone suggest the formation of a subsurface alloy according to our calculations.

4. Conclusions

In summary, we systematically studied the interaction and electronic

 310 properties of a graphene layer with $\text{Co}_x\text{Ir}_{1-x}/\text{Ir}(111)$ and $\text{Ir}/\text{Co}_x\text{Ir}_{1-x}/\text{Ir}(111)$ with variable Co concentration by DFT-D2 method. The computational results indicate that the surface alloy of $\text{Co}_x\text{Ir}_{1-x}$ on Ir(111) will remarkably enhance the corrugation of the graphene moiré superstructure, and this trend strengthens with the increase of x . In contrast, the subsurface alloy of

 315 $\text{Co}_x\text{Ir}_{1-x}$ in Ir(111) would suppress the geometrical corrugation and this effect is rather insensitive to the x value, leading to a relatively flat graphene mono-

layer. Accordingly, there is more charge accumulation between graphene and surface alloy, especially at the chemisorption region of gr/Co_xIr_{1-x}/Ir(111); the presence of the subsurface alloy slightly weakens the charge transfer between graphene and Ir surface layer due to the electronic structure effect. The analysis of stability suggests that at low Co concentration, the Co_xIr_{1-x} alloy prefers to exist on the subsurface underneath the gr/Ir interface bilayer to interact indirectly with the graphene layer; whereas at high Co concentration, Co_xIr_{1-x} alloy tends to segregate to the surface, thereby directly bonding with the graphene monolayer. This depends on the balance between the deformation of graphene and the interaction of graphene with the substrate. Our band structure calculation shows that the strong interaction of graphene with Co atoms destroys the Dirac cone; the formation of a subsurface Co-Ir alloy weakens the interaction between graphene and substrate and thereby makes the graphene layer more quasi freestanding with weak *p* doping. The results of our DFT calculations are supported by intensive ARPES measurements, which demonstrate that, when graphene is lying on a Co monolayer on Ir(111), the Dirac cone vanishes. The formation of subsurface Co-Ir alloy restores the presence of the Dirac cone at the Fermi level.

5. Acknowledgements

K. W. acknowledges the China Scholarship Council for the financial support. The computations were performed with resources provided by the North-German Supercomputing Alliance (HLRN) and computer facilities of the Freie Universität Berlin (ZEDAT).

340 **References**

- [1] K. S. Novoselov, A. K. Geim, S. V. Morozov, D. Jiang, M. I. Katsnelson, I. V. Grigorieva, S. V. Dubonos, A. A. Firsov, Two-dimensional gas of massless Dirac fermions in graphene, *Nature* 438 (7065) (2005) 197–200.
- [2] Y. Zhang, Y.-W. Tan, H. L. Stormer, P. Kim, Experimental observa-
345 tion of the quantum Hall effect and Berry’s phase in graphene, *Nature* 438 (7065) (2005) 201–204.
- [3] P. Pokharel, Q.-T. Truong, D. S. Lee, Multi-step microwave reduction of graphite oxide and its use in the formation of electrically conductive graphene/epoxy composites, *Compos. B. Eng.* 64 (C) (2014) 187–193.
- [4] A. A. Balandin, S. Ghosh, W. Bao, I. Calizo, D. Teweldebrhan, F. Miao, C. N. Lau, Superior thermal conductivity of single-layer graphene, *Nano Lett.* 8 (3) (2008) 902–907.
- [5] C. Lee, X. Wei, J. W. Kysar, J. Hone, Measurement of the elastic prop-
355 erties and intrinsic strength of monolayer graphene, *Science* 321 (2008) 385–388.
- [6] C. Berger, Z. Song, X. Li, X. Wu, N. Brown, C. Naud, D. Mayou, T. Li, J. Hass, A. N. Marchenkov, E. H. Conrad, P. N. First, W. A. de Heer, Electronic Confinement and Coherence in Patterned Epitaxial Graphene, *Science* 312 (5777) (2006) 1191–1196.
- [7] C. Berger, Z. Song, T. Li, X. Li, A. O. T. J. of, 2004, Ultrathin epitaxial
360 graphite: 2D electron gas properties and a route toward graphene-based nanoelectronics, *J. Phys. Chem. B* 108 (2004) 19912–19916.

- [8] K. V. Emtsev, A. Bostwick, K. Horn, J. Jobst, G. L. Kellogg, L. Ley, J. L. McChesney, T. Ohta, S. A. Reshanov, J. Röhl, E. Rotenberg, A. K. Schmid, D. Waldmann, H. B. Weber, T. Seyller, Towards wafer-size graphene layers by atmospheric pressure graphitization of silicon carbide, *Nat. Mater.* 8 (2009) 203–207.
- [9] D. R. Dreyer, S. Park, C. W. Bielawski, R. S. Ruoff, The chemistry of graphene oxide, *Chemical Society Reviews* 39 (1) (2009) 228–240.
- [10] Y. Hernandez, V. Nicolosi, M. Lotya, F. M. Blighe, Z. Sun, S. De, I. T. McGovern, B. Holland, M. Byrne, Y. K. Gun'Ko, J. J. Boland, P. Niraj, G. Duesberg, S. Krishnamurthy, R. Goodhue, J. Hutchison, V. Scardaci, A. C. Ferrari, J. N. Coleman, High-yield production of graphene by liquid-phase exfoliation of graphite, *Nature Nanotechnol.* 3 (9) (2008) 563–568.
- [11] Q. Yu, J. Lian, S. Siriponglert, H. Li, Y. P. Chen, S.-S. Pei, Graphene segregated on Ni surfaces and transferred to insulators, *Appl. Phys. Lett.* 93 (11) (2008) 113103.
- [12] X. Li, W. Cai, J. An, S. Kim, J. Nah, D. Yang, R. Piner, A. Velamakanni, I. Jung, E. Tutuc, S. K. Banerjee, L. Colombo, R. S. Ruoff, Large-area synthesis of high-quality and uniform graphene films on copper foils, *Science* 324 (2009) 1312–1314.
- [13] J.-H. Lee, E. K. Lee, W.-J. Joo, Y. Jang, B.-S. Kim, J. Y. Lim, S.-H. Choi, S. J. Ahn, J. R. Ahn, M.-H. Park, C.-W. Yang, B. L. Choi, S.-W. Hwang, D. Whang, Wafer-scale growth of single-crystal mono-

layer graphene on reusable hydrogen-terminated germanium, *Science* 344 (6181) (2014) 286–289.

[14] Y. S. Dedkov, E. Voloshina, Epitaxial graphene/Ge interfaces: a minireview, *Nanoscale* 12 (21) (2020) 11416–11426.

390 [15] S. Bae, H. Kim, Y. Lee, X. Xu, J.-S. Park, Y. Zheng, J. Balakrishnan, T. Lei, H. R. Kim, Y. Il Song, Y.-J. Kim, K. S. Kim, B. Özyilmaz, J.-H. Ahn, B. H. Hong, S. Iijima, Roll-to-roll production of 30-inch graphene films for transparent electrodes, *Nature Nanotechnol.* 5 (8) (2010) 574–578.

395 [16] J. Ryu, Y. Kim, D. Won, N. Kim, J. S. Park, E.-K. Lee, D. Cho, S.-P. Cho, S. J. Kim, G. H. Ryu, H.-A.-S. Shin, Z. Lee, B. H. Hong, S. Cho, Fast Synthesis of High-Performance Graphene Films by Hydrogen-Free Rapid Thermal Chemical Vapor Deposition, *ACS Nano* 8 (1) (2014) 950–956.

400 [17] M. Batzill, The surface science of graphene: Metal interfaces, CVD synthesis, nanoribbons, chemical modifications, and defects, *Surf. Sci. Rep.* 67 (3-4) (2012) 83–115.

[18] Y. S. Dedkov, E. Voloshina, M. Fonin, Scanning probe microscopy and spectroscopy of graphene on metals, *Phys. Status Solidi B* 252 (3) (2015) 451–468.
405

[19] Y. S. Dedkov, E. Voloshina, Graphene growth and properties on metal substrates, *J. Phys.: Condens. Matter* 27 (30) (2015) 303002.

- [20] M. Yang, Y. Liu, T. Fan, D. Zhang, Metal-graphene interfaces in epitaxial and bulk systems: A review, *Prog. Mater. Sci.* 110 (2020) 100652.
- 410 [21] J. Coraux, A. T. N'Diaye, M. Engler, C. Busse, D. Wall, N. Buckanie, F.-J. M. z. Heringdorf, R. van Gastel, B. Poelsema, T. Michely, Growth of graphene on Ir(111), *New J. Phys.* 11 (2009) 023006.
- [22] M. Kralj, I. Pletikosić, M. Petrović, P. Pervan, M. Milun, A. T. N'Diaye, C. Busse, T. Michely, J. Fujii, I. Vobornik, Graphene on Ir(111) characterized by angle-resolved photoemission, *Phys. Rev. B* 84 (7) (2011) 075427.
- 415 [23] C. Busse, P. Lazic, R. Djemour, J. Coraux, T. Gerber, N. Atodiresei, V. Caciuc, R. Brako, A. T. N'Diaye, S. Bluegel, J. Zegenhagen, T. Michely, Graphene on Ir(111): Physisorption with chemical modulation, *Phys. Rev. Lett.* 107 (3) (2011).
- 420 [24] E. Starodub, A. Bostwick, L. Moreschini, S. Nie, F. E. Gabaly, K. F. McCarty, E. Rotenberg, In-plane orientation effects on the electronic structure, stability, and Raman scattering of monolayer graphene on Ir(111), *Phys. Rev. B* 83 (12) (2011) 125428.
- 425 [25] I. Pletikosić, M. Kralj, M. Milun, P. Pervan, Finding the bare band: Electron coupling to two phonon modes in potassium-doped graphene on Ir(111), *Phys. Rev. B* 85 (15) (2012) 155447.
- [26] E. Voloshina, E. Fertitta, A. Garhofer, F. Mittendorfer, M. Fonin, A. Thissen, Y. S. Dedkov, Electronic structure and imaging contrast of graphene moiré on metals, *Sci. Rep.* 3 (2013) 1072.
- 430

- [27] S. Marchini, S. Günther, J. Wintterlin, Scanning tunneling microscopy of graphene on Ru(0001), *Phys. Rev. B* 76 (7) (2007) 075429.
- [28] B. Wang, S. Günther, J. Wintterlin, M. L. Bocquet, Periodicity, work function and reactivity of graphene on Ru(0001) from first principles, *New J. Phys.* 12 (4) (2010) 043041.
- [29] S. J. Altenburg, J. Kröger, B. Wang, M. L. Bocquet, N. Lorente, R. Berndt, Graphene on Ru(0001): Contact formation and chemical reactivity on the atomic scale, *Phys. Rev. Lett.* 105 (23) (2010) 236101.
- [30] E. Voloshina, N. Berdunov, Y. S. Dedkov, Restoring a nearly free-standing character of graphene on Ru(0001) by oxygen intercalation, *Sci. Rep.* 6 (2016) 20285.
- [31] E. Voloshina, Y. S. Dedkov, Atomic force spectroscopy and density-functional study of graphene corrugation on Ru(0001), *Phys. Rev. B* 93 (2016) 235418.
- [32] V. M. Karpan, G. Giovannetti, P. A. Khomyakov, Graphite and graphene as perfect spin filters, *Phys. Rev. Lett.* 99 (17) (2007) 176602.
- [33] Y. S. Dedkov, M. Fonin, Electronic and magnetic properties of the graphene–ferromagnet interface, *New J. Phys.* 12 (12) (2010) 125004.
- [34] E. Voloshina, R. Ovcharenko, A. Shulakov, Y. S. Dedkov, Theoretical description of X-ray absorption spectroscopy of the graphene-metal interfaces, *J. Chem. Phys.* 138 (15) (2013) 154706.

- [35] D. Marchenko, A. Varykhalov, J. Sánchez-Barriga, O. Rader, C. Carbone, G. Bihlmayer, Highly spin-polarized Dirac fermions at the graphene/Co interface, *Phys. Rev. B* 91 (23) (2015) 235431.
- 455 [36] D. Usachov, A. Fedorov, M. M. Otrokov, A. Chikina, O. Vilkov, A. Petukhov, A. G. Rybkin, Y. M. Koroteev, E. V. Chulkov, V. K. Adamchuk, A. Grüneis, C. Laubschat, D. V. Vyalikh, Observation of single-spin dirac fermions at the graphene/ferromagnet interface, *Nano Lett.* 15 (4) (2015) 2396–2401.
- 460 [37] S. Roche, J. Åkerman, B. Beschoten, J.-C. Charlier, M. Chshiev, S. P. Dash, B. Dlubak, J. Fabian, A. Fert, M. Guimarães, F. Guinea, I. Grigorieva, C. Schönberger, P. Seneor, C. Stampfer, S. O. Valenzuela, X. Waintal, B. van Wees, Graphene spintronics: the European Flagship perspective, *2D Mater.* 2 (3) (2015) 030202.
- 465 [38] H. Vita, S. Böttcher, K. Horn, E. Voloshina, Understanding the origin of band gap formation in graphene on metals: graphene on Cu/Ir(111), *Sci. Rep.* 4 (2014) 5704.
- [39] N. Rougemaille, A. T. N’Diaye, J. Coraux, C. Vo-Van, O. Fruchart, A. K. Schmid, Perpendicular magnetic anisotropy of cobalt films intercalated under graphene, *Appl. Phys. Lett.* 101 (14) (2012) 142403.
- 470 [40] R. Decker, J. Brede, N. Atodiresei, V. Caciuc, S. Blügel, R. Wiesendanger, Atomic-scale magnetism of cobalt-intercalated graphene, *Phys. Rev. B* 87 (4) (2013) 041403.

- [41] J. Coraux, A. T. N'Diaye, N. R. T. J. of, 2012, Air-protected epitaxial
475 graphene/ferromagnet hybrids prepared by chemical vapor deposition
and intercalation, *J. Phys. Chem. Lett.* 3 (2012) 2059–2063.
- [42] D. Alfè, M. Pozzo, E. Miniussi, S. Günther, P. Lacovig, S. Lizzit, R. Lar-
ciprete, B. S. Burgos, T. O. Mentş, A. Locatelli, A. Baraldi, Fine tuning
of graphene-metal adhesion by surface alloying, *Sci. Rep.* 3 (1) (2013)
480 2430.
- [43] E. Voloshina, B. Paulus, Y. S. Dedkov, Graphene layer morphology as
an indicator of the metal alloy formation at the interface, *J. Phys. Chem.*
Lett. 12 (2021) 19–25.
- [44] G. Kresse, J. Furthmuller, Efficiency of ab-initio total energy calcula-
485 tions for metals and semiconductors using a plane-wave basis set, *Comp.*
Mater. Sci. 6 (1) (1996) 15–50.
- [45] G. Kresse, J. Hafner, Norm-conserving and ultrasoft pseudopotentials
for first-row and transition-elements, *J. Phys.: Condens. Matter* 6 (40)
(1994) 8245–8257.
- 490 [46] G. Kresse, J. Hafner, Ab initio molecular dynamics for liquid metals,
Phys. Rev. B 47 (1) (1993) 558–561.
- [47] J. P. Perdew, K. Burke, M. Ernzerhof, Generalized gradient approxima-
tion made simple, *Phys. Rev. Lett.* 77 (18) (1996) 3865–3868.
- [48] S. Grimme, Semiempirical GGA-type density functional constructed
495 with a long-range dispersion correction, *J. Comput. Chem.* 27 (15)
(2006) 1787–1799.

- [49] P. E. Blöchl, Projector augmented-wave method, *Phys. Rev. B* 50 (24) (1994) 17953–17979.
- [50] J. Tersoff, D. R. Hamann, Theory of the scanning tunneling microscope, *Phys. Rev. B* 31 (2) (1985) 805–813.
- 500 [51] P. V. C. Medeiros, S. Stafström, J. Björk, Effects of extrinsic and intrinsic perturbations on the electronic structure of graphene: Retaining an effective primitive cell band structure by band unfolding, *Phys. Rev. B* 89 (4) (2014) 041407.
- 505 [52] P. V. C. Medeiros, S. S. Tsirkin, S. Stafström, J. Björk, Unfolding spinor wave functions and expectation values of general operators: Introducing the unfolding-density operator, *Phys. Rev. B* 91 (4) (2015) 041116(R).
- [53] J. Coraux, A. T. N Diaye, C. Busse, T. Michely, Structural coherency of graphene on Ir(111), *Nano Lett.* 8 (2) (2008) 565–570.
- 510 [54] T. Vincent, E. Voloshina, S. Pons, S. Simon, M. Fonin, K. Wang, B. Paulus, D. Roditchev, Y. S. Dedkov, S. Vlaic, Quantum well states for graphene spin-texture engineering, *J. Phys. Chem. Lett.* 11 (2020) 1594–1600.
- [55] Y. S. Dedkov, E. Voloshina, Spectroscopic and DFT studies of graphene intercalation systems on metals, *J. Electron. Spectrosc. Relat. Phenom.* 219 (2017) 77–85.
- 515 [56] H. Tetlow, J. P. de Boer, I. J. Ford, D. D. Vvedensky, J. Coraux, L. Kantorovich, Growth of epitaxial graphene: Theory and experiment, *Phys. Rep.* 542 (3) (2014) 195–295.

- 520 [57] S. Vlaic, A. Kimouche, J. Coraux, B. Santos, A. Locatelli, N. Rougemaille, Cobalt intercalation at the graphene/iridium(111) interface: Influence of rotational domains, wrinkles, and atomic steps, *Appl. Phys. Lett.* 104 (10) (2014) 101602.
- [58] S. Vlaic, N. Rougemaille, A. Kimouche, B. S. Burgos, A. Locatelli,
525 J. Coraux, Intercalating cobalt between graphene and iridium (111): Spatially dependent kinetics from the edges, *Phys. Rev. Materials* 1 (5) (2017) 053406.
- [59] J. Drnec, S. Vlaic, I. Carlomagno, C. J. Gonzalez, H. Isern, F. Carlà,
530 R. Fiala, N. Rougemaille, J. Coraux, R. Felici, Surface alloying upon Co intercalation between graphene and Ir(111), *Carbon* 94 (C) (2015) 554–559.
- [60] I. Carlomagno, J. Drnec, A. M. Scaparro, S. Cicia, S. Vlaic, R. Felici, C. Meneghini, Co-Ir interface alloying induced by thermal annealing, *J. Appl. Phys.* 120 (19) (2016) 195302.
- 535 [61] S. Vlaic, N. Rougemaille, A. Artaud, V. T. Renard, L. Huder, J.-L. Rouviere, A. Kimouche, B. Santos, A. Locatelli, V. Guisset, P. David, C. Chapelier, L. Magaud, B. Canals, J. Coraux, Graphene as a mechanically active, deformable two-dimensional surfactant, *J. Phys. Chem. Lett.* 9 (2018) 2523–2531.
- 540 [62] I. Pletikosić, M. Kralj, P. Pervan, R. Brako, J. Coraux, A. T. N’Diaye, C. Busse, T. Michely, Dirac cones and minigaps for graphene on Ir(111), *Phys. Rev. Lett.* 102 (5) (2009) 056808.

- 545 [63] I. Pletikosić, M. Kralj, D. Sokcevic, R. Brako, P. Lazić, P. Pervan, Photoemission and density functional theory study of Ir(111); energy band gap mapping, *J. Phys.: Condens. Matter* 22 (13) (2010) 135006.
- [64] S. Rusponi, M. Papagno, P. Moras, S. Vlaic, M. Etzkorn, P. M. Sheverdyeva, D. Pacilé, H. Brune, C. Carbone, Highly anisotropic Dirac cones in epitaxial graphene modulated by an island superlattice, *Phys. Rev. Lett.* 105 (24) (2010) 246803.

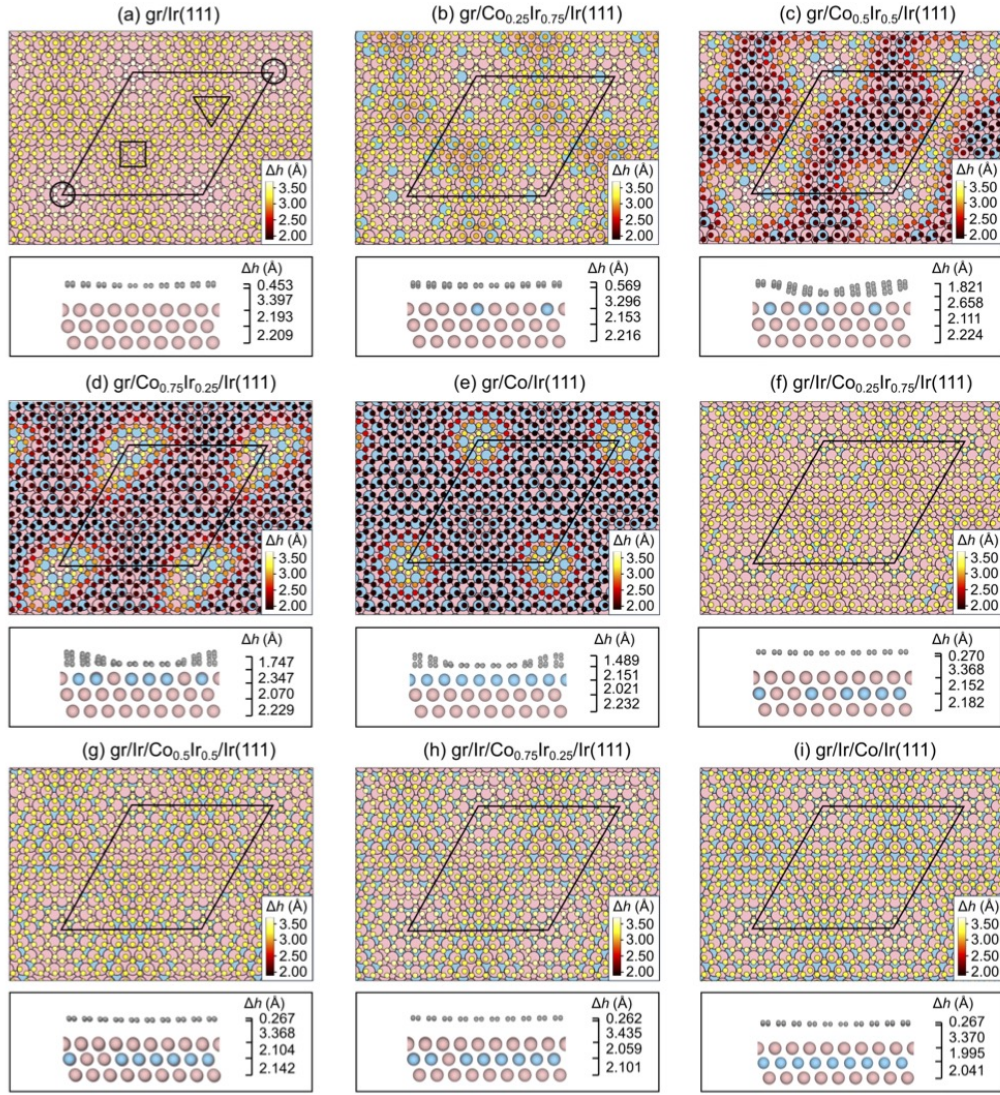


Figure 1: Structural models of (a)-(e) Gr/Co_xIr_{1-x}/Ir(111) and (f)-(i) Gr/Ir/Co_xIr_{1-x}/Ir(111) with $x=0.00, 0.25, 0.50, 0.75$ and 1.00 . The color scale indicates the heights measured from the first layer of the substrate. The black rhombus marks the unit cell of the considered system. Ir and Co atoms are shown in pink and blue, respectively. The high-symmetry places in (a) are marked by circle, square, and triangle for ATOP, FCC, and HCP, respectively.

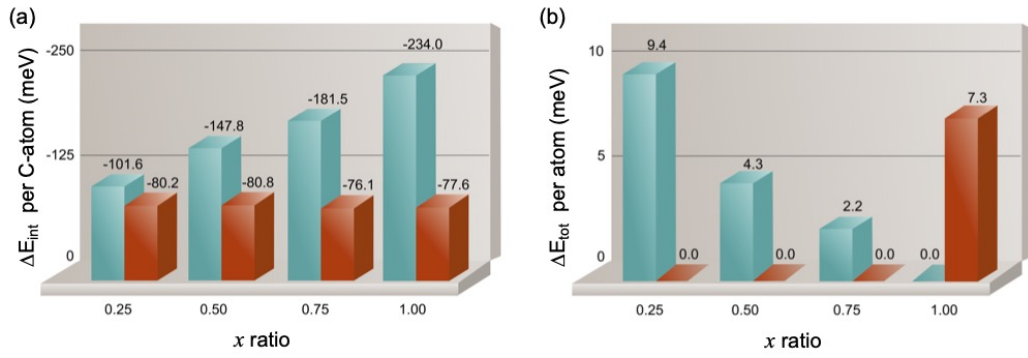


Figure 2: (a) The interaction energy (ΔE_{int}) per C-atom as a function of x ratio for $\text{gr}/\text{Co}_x\text{Ir}_{1-x}/\text{Ir}(111)$ (blue) and $\text{gr}/\text{Ir}/\text{Co}_x\text{Ir}_{1-x}/\text{Ir}(111)$ (red). (b) The total energy difference (ΔE_{tot}) per atom as a function of x ratio for $\text{gr}/\text{Co}_x\text{Ir}_{1-x}/\text{Ir}(111)$ (blue) and $\text{gr}/\text{Ir}/\text{Co}_x\text{Ir}_{1-x}/\text{Ir}(111)$ (red).

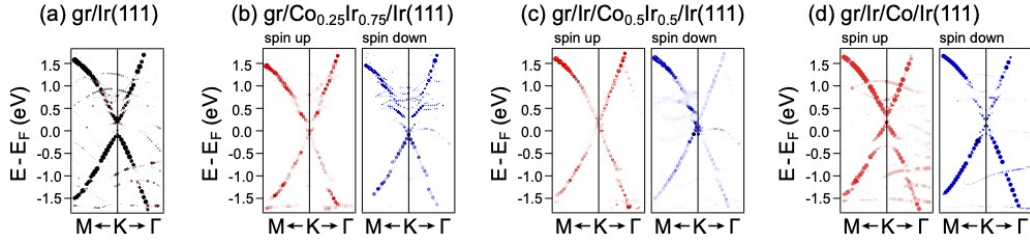


Figure 3: Band structures of (a) gr/Ir(111), (b) gr/Co_{0.25}Ir_{0.75}/Ir(111), (c) gr/Ir/Co_{0.5}Ir_{0.5}/Ir(111) and (d) gr/Ir/Co/Ir(111) in the vicinity of the K point obtained after the unfolding procedure for the graphene (1×1) primitive cell. Spin-up (red) and spin-down (blue) states are shown in (b)-(d).

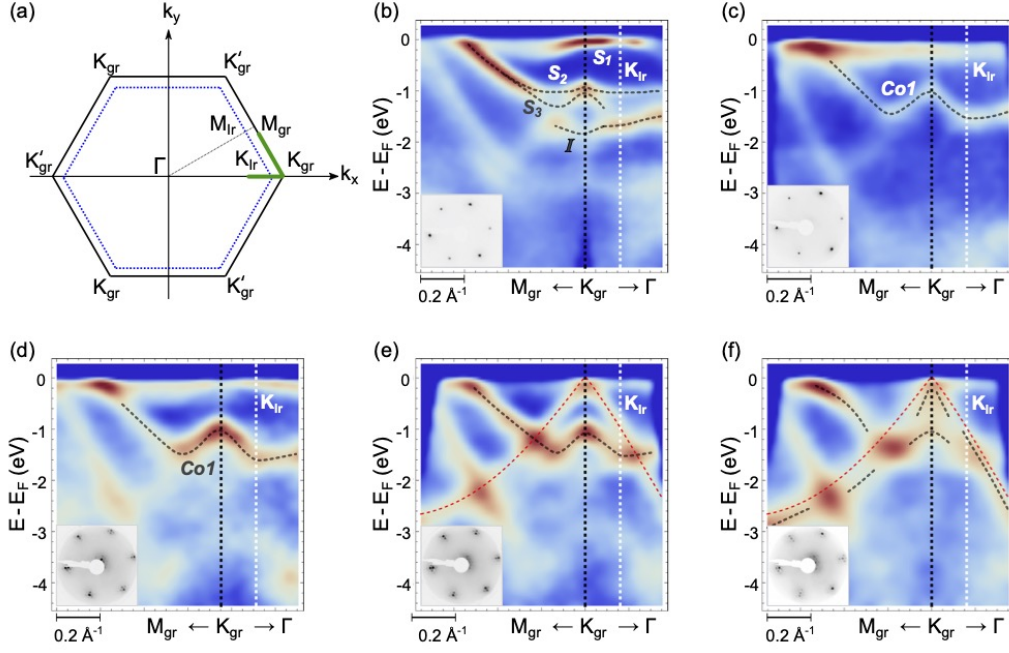


Figure 4: (a) Schematic representation of the gr and Ir(111) Brillouin zones. The green thick line highlight the M_{gr} - K_{gr} - Γ direction in reciprocal space used for the electronic dispersion shown in (b)-(f). Electronic band dispersions obtained in ARPES experiments for (b) the Ir(111) surface, (c) single Co layer on Ir(111), (d) gr/Co_{1ML}/Ir, (e) gr/Co_{0.5ML}/Ir(111) and (f) gr/Co-Ir alloy obtained by annealing the sample shown in (e) to 873K. The grey dashed lines highlight the band dispersion in each sample. The red dashed line shows a tight binding fit up to three nearest neighbour of gr/Ir(111). Insets shows the LEED pattern of the corresponding sample.